

# Improved Gold Nanoprobes for Detection of Single Nucleotide Polymorphisms: The Influence of Size

Maria Enea, Miguel Peixoto de Almeida, André Dias, Beatriz Ferreira, Carlos Bernardes, Orfeu Flores, Eulália Pereira, and Ricardo Franco\*

Gold nanoparticles (AuNPs) are widely used in biomedical diagnostics due to their unique plasmonic properties, with larger AuNPs showing higher extinction coefficients for the plasmon band and, consequently, more intense colors than the more commonly used spherical 20 nm AuNPs. Other factors can be important in the performance of different-sized AuNPs, including surface area, colloidal stability, and curvature effects. Here, the properties of spherical 20 nm AuNPs and 35 nm AuNPs functionalized with a specific thiol-modified oligonucleotide–Au nanoprobes are compared when used on a colorimetric assay for the detection of a single nucleotide polymorphism related to lactose intolerance in humans. Successful functionalization of AuNPs is assessed by UV–vis spectroscopy, agarose gel electrophoresis, dynamic and electrophoretic light scattering, and nanoparticle tracking analysis. Statistical differences between Au-nanoprobe DNA target groups are calculated using analysis of variance and a post hoc Tukey's test. These results show that both 35 and 20 nm Au nanoprobes have similar detection limits using a 0.15 nmol dm<sup>-3</sup> nanoprobe concentration compared to 2.5 nmol dm<sup>-3</sup>. Interestingly, the use of 35 nm Au nanoprobes allows a reduction of 80% and 48% in the amount of gold and oligonucleotide used in the assay, respectively.

## 1. Introduction

Gold nanoparticles (AuNPs) present attractive nanoscale properties including a high surface area to volume ratio, high colloidal stability, easy functionalization, and intense visible light absorption and scattering.<sup>[1,2]</sup> These properties make them particularly useful for the development of colorimetric molecular assays for biological molecules such as proteins and nucleic acids.<sup>[2–5]</sup> In this context, functionalized AuNPs with single-stranded thiolated DNA are excellent probes for sensitive colorimetric detection of specific DNA sequences, using a non-cross-linking format.<sup>[2,4–6]</sup> Although the highly sensitive cross-linking approach was proposed in the late 1990s by the pioneering C.A. Mirkin research group,<sup>[5]</sup> the fact that two different single-stranded thiolated DNA probes need to be used and separately optimized, associated with stability issues, has hindered its further development.

One of the most challenging applications of this methodology is detecting single nucleotide polymorphisms (SNPs).<sup>[6–8]</sup> SNPs are associated with disease phenotype and other relevant clinical and environmental factors. Their detection is important as a diagnostic tool for many diseases, but also very challenging, as it usually requires highly sensitive and expensive methods. One example is the detection of SNPs associated with lactose intolerance or adult-type hypolactasia. This condition is characterized by a genetically determined inability to digest significant amounts of lactose and it is widely spread in the European population.<sup>[9,10]</sup> The associated SNP, 13910C/T, is located within the gene MCM6, ≈14 kb upstream of the lactase gene (LCT), responsible for producing the enzyme lactase that degrades lactose. Mutation in the MCM6 gene directly affects the LCT, and therefore, lactase production. Individuals with one or both copies of the T allele (C/T or T/T) at this locus can digest lactose, whereas individuals with no copy of the T allele (C/C) are incapable of digesting lactose.<sup>[11,12]</sup>


The detection of SNPs using Au nanoprobes can be performed using the non-cross-linking method. Detection is based on the visible change of color from red to blue, upon conversion of Au nanoprobes from a dispersed to an aggregated state upon salt addition. For samples containing non-complementary/mismatch targets, salt addition induces

M. Enea, A. Dias, R. Franco  
 Associate Laboratory i4HB – Institute for Health and Bioeconomy  
 Faculdade de Ciências e Tecnologia, Universidade NOVA de Lisboa  
 Caparica 2829-516, Portugal  
 E-mail: rft@fct.unl.pt

M. Enea, A. Dias, R. Franco  
 UCIBIO – Applied Molecular Biosciences Unit  
 Departamento de Química  
 Faculdade de Ciências e Tecnologia da Universidade NOVA de Lisboa  
 Caparica 2829-516, Portugal

M. Peixoto de Almeida, B. Ferreira, E. Pereira  
 REQUIMTE/LAQV  
 Departamento de Química e Bioquímica  
 Faculdade de Ciências da Universidade do Porto  
 Porto 4169-007, Portugal

C. Bernardes, O. Flores  
 STABVIDA  
 Investigação e Serviços em Ciências Biológicas Lda  
 Madan Parque, Caparica 2825-182, Portugal

 The ORCID identification number(s) for the author(s) of this article can be found under <https://doi.org/10.1002/ppsc.202200137>.

© 2022 The Authors. Particle & Particle Systems Characterization published by Wiley-VCH GmbH. This is an open access article under the terms of the Creative Commons Attribution-NonCommercial License, which permits use, distribution and reproduction in any medium, provided the original work is properly cited and is not used for commercial purposes.

DOI: 10.1002/ppsc.202200137

aggregation, with a characteristic change of color. Conversely, when a complementary target hybridizes with the oligonucleotides in the Au nanoprobe, they become shielded from salt-induced aggregation, and the solution maintains its original red color. This method is very simple and effective for the detection of DNA target sequences since the change in color can be easily detected visually or using a spectrophotometer.<sup>[6,13–17]</sup> For SNPs, the detection is more difficult, as mutated samples partially hybridize with the oligos in the probe, thus, providing intermediate shielding from salt-induced aggregation, in comparison with non-complementary and complementary samples. In this case, the difference in optical properties between positive and mutated samples is more subtle, and visual detection is not possible. Nevertheless, using this method, an SNP in the fat mass and obesity-associated gene could be detected. Spherical 14 nm-AuNP was used with a detection sensitivity as low as 20  $\mu\text{g mL}^{-1}$  for the homozygous polymerase chain reaction (PCR) samples, while heterozygous PCR samples afforded a detection sensitivity of 30  $\mu\text{g mL}^{-1}$ .<sup>[8]</sup>

Several procedures were reported to optimize the performance of this type of AuNPs-based assays. Several features of the oligonucleotides in the Au nanoprobe can be optimized, including the type and length of spacers between the thiol group and the recognition sequence, the position of the mismatch, and the functionalization procedure.<sup>[6]</sup> Doria et al. established that optimal hybridization density for SNP discrimination at room temperature is obtained at  $83 \pm 4$  thiol-oligonucleotides per 13.5 nm AuNP and with the mismatch located at the 3'-end of the oligonucleotide.<sup>[6]</sup> The use of a spacer between the thiol group and the nucleotide is also recommended, as it moves the recognition sequence further from the particle surface and prevents steric hindrance upon target hybridization.<sup>[7,18,19]</sup> This modification improves DNA loading, while overall decreasing the interaction of DNA bases with Au, and therefore, their tendency to lie on the nanoparticle surface.<sup>[19]</sup>

Two highly efficient functionalization methods of Au nanoprobe are known: the pH method<sup>[20,21]</sup> and the well-established salt-aging method.<sup>[22]</sup> The latter has been extensively used for the 15 nm AuNPs but proved to be challenging for larger AuNPs for which the pH method seems to be more effective.<sup>[20–22]</sup>

One possible way to further improve the detection sensitivity and discrimination of this method, which can be particularly useful for SNPs detection, is to change the optical and aggregation properties of AuNPs. Both these properties are highly affected by the size and shape of AuNPs. In particular, AuNPs of larger sizes are expected to increase detection sensitivity due to: i) higher extinction coefficients, translated into a more intense color for lower AuNPs concentrations; and ii) lower AuNP curvatures enabling more interactions with the target.<sup>[20]</sup> Nevertheless, there is a lack of studies comparing the influence of the size of AuNPs in the detection process, and most of the published work focused on the use of AuNPs around 15–20 nm, ignoring the high potential of larger AuNPs. Therefore, the present work is focused on developing Au nanoprobe for the optical detection of SNPs through a comparison study between two different-sized spherical AuNPs: the well-established 20 nm-AuNPs and the less-explored 35 nm-AuNPs. For this purpose, AuNPs were functionalized with a thiol-modified oligonucleotide using both the salt-aging method and the pH method. The performance of the obtained Au nanoprobe in detecting the SNP associated with lactose intolerance was evaluated through a non-cross-linking approach using synthetic DNA targets with two distinct lengths: 40 and 120 bp.

## 2. Results and Discussion

To study the influence of nanoparticle size, we have used the detection scheme depicted in **Figure 1**. The 20-mer oligonucleotide used to functionalize AuNPs is totally complementary to the DNA sequence of lactose intolerance (13910\**C* SNP) and

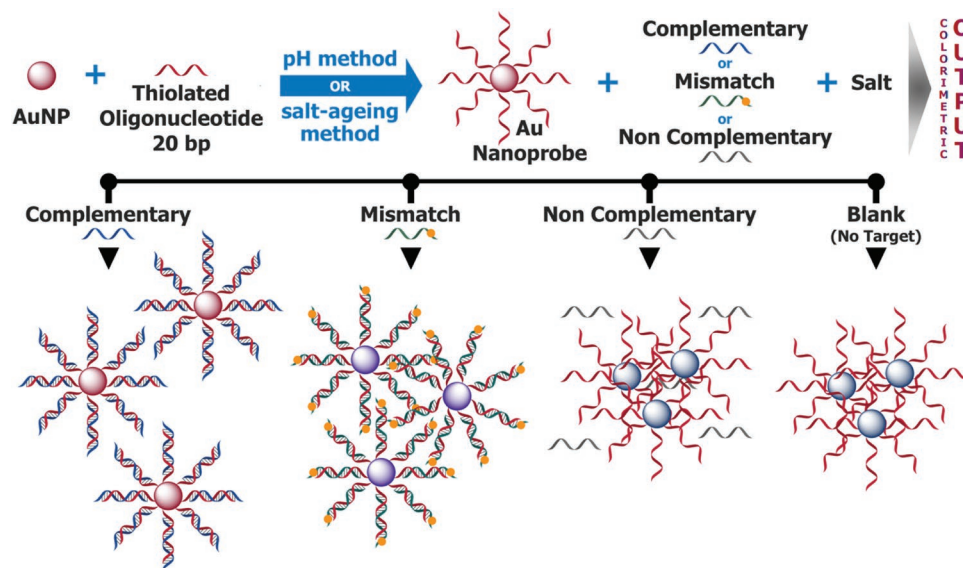


**Figure 1.** SNP detection assay based on the state of aggregation of Au nanoprobe in the presence of target DNA that is complementary, mismatched, noncomplementary (Negative Control), or its absence (Blank) after the addition of salt.

partially complementary to the DNA sequence of lactose tolerance (13910\*T SNP). Au nanoprobe were hybridized to DNA targets and controls, and after hybridization, the resistance to salt-induced aggregation was assessed by UV/vis spectroscopy. The expected outcome is the following: i) Upon hybridization with totally complementary DNA (CC), Au nanoprobe become resistant to salt-induced aggregation, so no significant changes are detected in the plasmon band. ii) For the negative control (non-complementary DNA) and the blank (absence of DNA target), Au nanoprobe aggregate upon salt addition. The solution changes its color from red to blue, due to the appearance of a new localized surface plasmon resonance (LSPR) band at higher wavelengths ( $\approx 650$  nm). iii) For the partially complementary DNA (mismatch or TT), intermediate behavior is expected, with partial aggregation of the DNA probes. In this case, an LSPR band at  $\approx 650$  nm is detected, with a lower intensity than the fully aggregated samples. The degree of aggregation can be assessed by the ratio between absorbance at the wavelength corresponding to the LSPR of the aggregates and the absorbance at the wavelength of the LSPR of non-aggregated Au nanoprobe.

Since the expected results for mismatched DNA samples correspond to partial aggregation of the Au nanoprobe, it is critical that the Au nanoprobe used do not show any significant aggregation. When the Au nanoprobe solution used contains even a low amount of aggregates, discrimination of complementary and mismatch samples is significantly impaired. Thus, our first step was to evaluate the aggregation state of Au nanoprobe using different functionalization methods. We have also tried a cross-linking approach to perform this assay, with unsuccessful results.

This type of assay uses two Au nanoprobe (a 3'- and a 5'-thiolated), which hybridize with consecutive portions of the target. Cross-linking of the Au nanoprobe brings the AuNPs into close vicinity, resulting in a color change of the solution from red to blue. For both AuNP sizes, the cross-linking assays did not result in Au-nanoprobe aggregation when using

the complementary and mutated ssDNA targets (results not shown). Since Au nanoprobe obtained using the 5' thiolated-oligonucleotide had already been proven to be functioning correctly in the non-cross-linking assay, we concluded that further optimization of the 3' thiolated-oligonucleotide was needed, and will be tried in future work.

## 2.1. Functionalization and Assay Development for the 20 and 35 nm Au Nanoprobe

### 2.1.1. Functionalization of the 20 and 35 nm AuNPs

Functionalization of AuNPs with thiol-modified oligonucleotides has been the subject of several studies. In order to optimize the degree of functionalization and the availability of the DNA bases for hybridization, two methods based on the decrease of the electrostatic repulsion between oligonucleotides have been proposed: i) the salt aging (SA) method,<sup>[8,22–24]</sup> and the pH method.<sup>[20,21,25]</sup> In both methods, the neutralization of oligonucleotide charge with the consequent decrease in surface charge of the functionalized nanoprobe, can lead to partial aggregation. This is particularly important for larger nanoparticles, which are intrinsically more prone to aggregation.<sup>[20,21,26]</sup>

Here, both the SA and the pH methods were used for the functionalization of 20 and 35 nm AuNPs with different molar ratios of a thiol-modified 20-mer oligonucleotide. The state of aggregation of the resulting probes was assessed by UV/vis spectroscopy (Figure 2).

The application of the SA method to 35 nm AuNPs at low oligonucleotide:AuNPs ratios (<2000) always resulted in extensive aggregation. These results agree with those reported by Valentini et al. that confirmed the need for a high oligonucleotide: AuNPs ratio (>2000) for a successful functionalization of 35 nm AuNPs using the SA method,<sup>[26]</sup> therefore, the pH method was preferred as it produces stable nanoprobe at

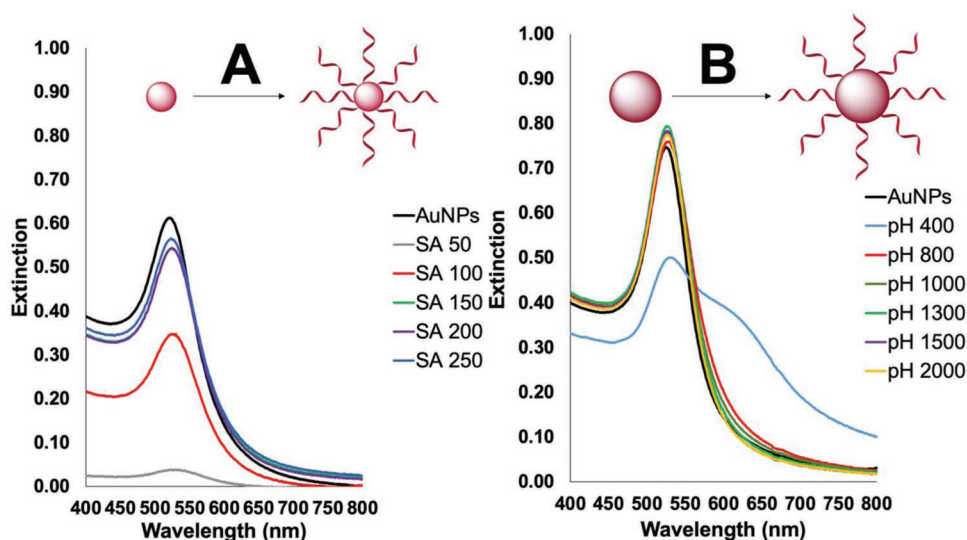


**Figure 2.** UV–vis spectra of A) 20 nm AuNPs functionalized by the salt aging method using molar ratios of oligo/AuNPs between 50 and 250; and B) 35 nm AuNPs functionalized by the pH method using molar ratios of oligo/AuNPs between 400 and 2000. In panels (A) and (B), the black line is the spectrum for the respective non-functionalized AuNPs.

low oligonucleotide:AuNPs ratios. For the smaller 20 nm Au nanoprobess, both functionalization methods yielded non-aggregated, stable nanoprobess. Since the results for the discrimination of SNPs were slightly better using 20 nm Au nanoprobess functionalized by the SA method, these were chosen for further studies (Figure S3, Supporting Information).

UV-vis spectra of the synthesized AuNPs are represented as black lines in Figure 2. 20 nm AuNPs show an LSPR band centered around 520 nm, as expected for spherical AuNP of this size (Figure 2A).<sup>[6,8]</sup> On the other hand, 35 nm AuNPs have an LSPR band centered at a higher wavelength,  $\approx 528$  nm, as expected due to the larger size.<sup>[27]</sup> In both cases, no other bands are present, indicating the absence of aggregates. The spectra of the functionalized AuNPs are shown as colored lines in Figure 2. It can be noticed that the oligonucleotide:AuNP ratio of 50 and 100 for the salt aging method applied to 20 nm AuNPs (Figure 2A), and the oligonucleotide:AuNP ratio 400 for the pH method applied to 35 nm (Figure 2B), resulted in low extinction and/or presence of secondary extinction bands at higher wavelengths, indicating an inefficient functionalization process and significant aggregation and/or loss of AuNPs during the procedure.<sup>[28]</sup> In the case of 20 nm AuNPs (Figure 2A), the shape and location of UV-vis spectra for ratios 150, 200, and 250 indicate that the functionalization was successful as no aggregation or significant loss of AuNPs occurred during the process. A small shift in the maximum extinction wavelength from 520 to 524 nm can be attributed to the adsorption of the oligonucleotide.<sup>[5,7]</sup> In the case of 35 nm AuNPs (Figure 2B), functionalization with an oligonucleotide:AuNP ratio of 800 or higher seems promising without signs of aggregation.

Hydrodynamic diameter ( $D_H$ ) measurements by dynamic light scattering, zeta potential measurements by electrophoretic light scattering, and agarose gel electrophoretic analysis confirm the results obtained by UV-vis (Supporting Information). All these techniques are sensitive to the formation of aggregates, but only for the formation of very large aggregates or

extensive aggregation of the nanoparticles. For the discrimination of small-sized aggregates and slightly aggregated samples, nanoparticle tracking analysis (NTA) is a more reliable technique. This technique records on video the Brownian motion of individual nanoparticles, providing the simultaneous measurement of the  $D_H$  of multiple nanoparticles in the sample. 20 nm AuNPs could not be assessed by NTA, since their size is below the detection limit of the technique. Figure 3 shows the  $D_H$  histograms of the parental 35 nm AuNPs before functionalization with oligonucleotides, and gold nanoprobess obtained after functionalization with oligonucleotide:AuNP ratios of 500, 900, and 1300.

Except for the sample with an oligonucleotide:AuNP ratio of 500, the samples analyzed have only one major population centered at  $D_H$  values of 30 nm before functionalization and 32 nm after functionalization. For an oligonucleotide:AuNP ratio of 500, two peaks at 39 and 48 nm with similar populations are observed. In addition, several other minor populations centered at higher  $D_H$  values are detected. It should be noted that for AuNPs, the minor population with higher  $D_H$  is centered at 120 nm, which, based on the main peak  $D_H$  of the pristine AuNPs corresponds to the formation of aggregates with up to four nanoparticles. For all the functionalized Au nanoprobess, the minor populations have  $D_H$  values below 115 nm, which may correspond to the formation of aggregates of 2–4 nanoparticles. These results strongly indicate that the functionalization process induces aggregation of the nanoparticles for the lower ratio studied (500), with two main populations and large size distribution. For the higher ratios studied (900 and 1300), the functionalized AuNPs have higher colloidal stability with only a minor population of dimers and higher oligomers.

Considering these results, we selected oligonucleotide:AuNPs ratios of 150 for 20 nm AuNPs and 1300 for 35 nm AuNPs, for further studies. These values are in the range of published data for the functionalization of spherical AuNPs below 15 nm.<sup>[14,29]</sup> Regarding the functionalization of the larger 35 nm AuNPs, the

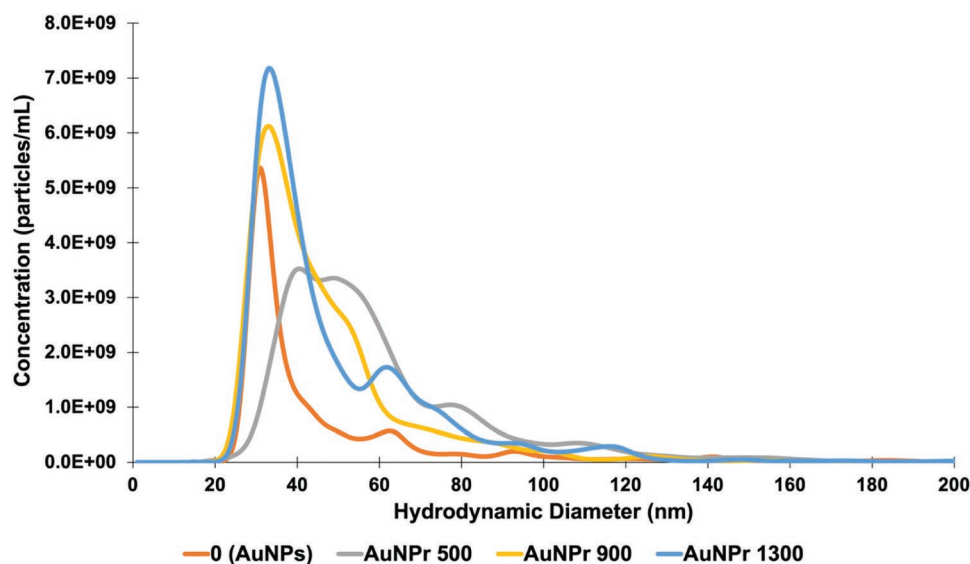


**Figure 3.** Size distribution of 35 nm AuNPs (red) and the corresponding nanoprobess prepared with three different AuNPs:oligonucleotide ratios (gray – 500; yellow – 900; blue – 1300), obtained by nanoparticle tracking analysis (NTA).

need for a higher ratio was expected, as higher diameters correspond to a higher available surface area and the selected ratio is within the range of previous reports.<sup>[19,20]</sup> The use of Au nanoprobe with larger sizes is associated with a decrease in curvature, affecting the interactions among the DNA strands, and consequently affecting the DNA density/loading on the surface of AuNPs.<sup>[19]</sup>

To obtain Au nanoprobe that are effective in diagnostic assays, it is necessary to guarantee oligonucleotide:AuNP ratios, which are sufficiently high to ensure good colloidal stability of the Au nanoprobe, but low enough to ensure an efficient hybridization with the DNA target.<sup>[30]</sup> The ratio selected in our study for the 20 nm AuNPs corresponds to 21 pmol<sub>ssDNA</sub> cm<sup>-2</sup> and it is slightly lower than that found by Doria et al. (24 pmol<sub>ssDNA</sub> cm<sup>-2</sup>) for 13.5 nm AuNPs<sup>[6]</sup> and by Song et al. for 20 nm Au nanoprobe (2830 pmol cm<sup>-2</sup>)<sup>[30]</sup> leading to the high stability of the nanoprobe and the duplex formed with the complementary sequence. For the 35 nm AuNPs, the ratios 1:500, 1:900, and 1:1300 correspond to 21, 37, and 53 pmol<sub>ssDNA</sub> cm<sup>-2</sup>, respectively. Clearly, using 21 pmol<sub>ssDNA</sub> cm<sup>-2</sup> for larger AuNPs is not enough to provide a homogeneous distribution of  $D_H$ . The need for higher oligonucleotide:nanoparticle ratios for larger nanoparticles indicates that curvature effects are also important for establishing the best functionalization ratios, and they should be taken into consideration when preparing optimized Au nanoprobe.

## 2.2. Non-Cross-Linking Detection of an SNP Associated with Lactose Intolerance

Figure S8, Supporting Information, summarizes UV-vis spectra for the 35 nm Au nanoprobe in the presence (Complementary/Mismatch/Negative Control) or absence (Au nanoprobe, Blank) of DNA targets and after MgCl<sub>2</sub> induced aggregation. The basis of this SNP detection method is the appearance of a second plasmon band at higher wavelengths upon salt-induced aggregation (Figure 1). Resistance to aggregation is different in the presence of the DNA target that is totally or partially complementary to the Au nanoprobe functionalizing oligonucleotide. Upon hybridization with the totally complementary target, the resulting Au nanoprobe become very resistant to aggregation. In this case, the optical properties remain similar to those of the probes before salt addition, that is, the solution stays red, with a shift of the plasmon band from 528 to 553 nm, due to DNA hybridization to the Au nanoprobe (Figure S8, Supporting Information). In contrast, if the DNA target is noncomplementary or absent, it will not hybridize to any part of the oligonucleotide from the Au nanoprobe, and no protection will occur against salt-induced aggregation. The solution turns blue-purple, and an additional plasmon band appears at ≈650 nm. Hybridization with a partially complementary DNA affords incomplete protection from aggregation, translated into a significant LSPR redshift (574 nm) along with an increase in bandwidth. Such an effect is related to a decrease in the amount of DNA at the surface of Au nanoprobe.

The extent of aggregation of AuNPs can be easily assessed by UV/vis spectrophotometry, either directly by the extinction of the LSPR band of the aggregates or by calculating extinction

ratios.<sup>[6–8,31,32]</sup> A ratio frequently used in this type of study is calculated as LSPR maximum absorptions of the non-aggregated versus aggregated nanoparticles,  $Abs_{Non-Agg}/Abs_{Agg}$ .<sup>[8,31,33–38]</sup> For instance, these types of ratios were previously used for ≈14 and ≈35 nm spherical AuNPs as  $Abs_{525nm}/Abs_{585nm}$  and  $Abs_{542nm}/Abs_{700nm}$ , respectively.<sup>[31,33]</sup> Based on UV-vis spectra from the examples in Figure S8, Supporting Information, a higher ratio is expected for the Au nanoprobe hybridized with a fully complementary DNA compared to hybridization with a mismatched DNA, corresponding to differences in their aggregation profile. The Au nanoprobe containing mismatched DNA would have a lower ratio, as the formed duplex is less stable and consequently suffers partial aggregation after salt addition. The use of these ratios is very useful but does not take into consideration the fact that the aggregation pattern of Au nanoprobe changes depending on the AuNP size, the salt employed to induce the aggregation process, and the length of the DNA target. Therefore, the subtraction of the non-aggregated sample spectrum from the aggregated sample spectrum for each type of AuNPs would give the minimum and maximum absorption wavelengths corresponding to a precise location of the non-aggregated and aggregated peaks, respectively, that can then be used to calculate  $Abs_{Non-Agg}/Abs_{Agg}$  ratios. Here, we have used ratios calculated in this way, as a measurement of Au nanoprobe aggregation, with higher ratios meaning less aggregation, thus corresponding to a more extensive hybridization between the oligo on the Au nanoprobe and the target DNA.

Synthetic DNA is often preferred for optimization and/or mechanistical studies due to the cost reduction and flexibility in changing the experimental conditions, in contrast with the biological samples, as PCR products, where the required experimental conditions can limit the sensitivity of the detection assay.<sup>[6–8,30,39]</sup> One of these specific conditions is the high temperature (95 °C) required for dsDNA denaturation, which can affect the stability of the Au nanoprobe and the recently formed DNA duplex. With synthetic ssDNA targets, the annealing process can be performed at lower temperatures, even room temperature, avoiding interferences with Au nanoprobe and denaturation of the newly formed duplex.<sup>[7,30]</sup> Here, we have used a temperature close to the melting temperature of the DNA samples, ensuring an optimal hybridization between the oligo on the Au nanoprobe and DNA targets.

$Abs_{Non-Agg}/Abs_{Agg}$  ratios for DNA target concentrations up to 100 ng μL<sup>-1</sup> were measured for assays with complementary, mismatched, and negative control samples. Two DNA targets were used, namely a 40-mer target (Figure 4); and a 120-mer target (Figure 5), to assess the influence of target length on the outcome of the assay. This is important because real-life PCR-derived samples are usually longer than 40 bp. For example, in similar non-cross-linking 20 nm Au nanoprobe-based colorimetric assays for SNPs detection, ≈400<sup>[13]</sup> or ≈225 bp<sup>[8]</sup> PCR fragments were used. For each DNA target, both 20- and 35-nm AuNPs were used to synthesize Au nanoprobe using a 20-mer thiol-modified oligonucleotide. For sequences of targets and probe oligonucleotides, see Table 2 in Experimental Section.

A concentration-dependent protection against aggregation can be noticed for both the complementary and the mismatched samples with an increase of the corresponding  $Abs_{Non-Agg}/Abs_{Agg}$  (black and green lines, respectively, Figures 4

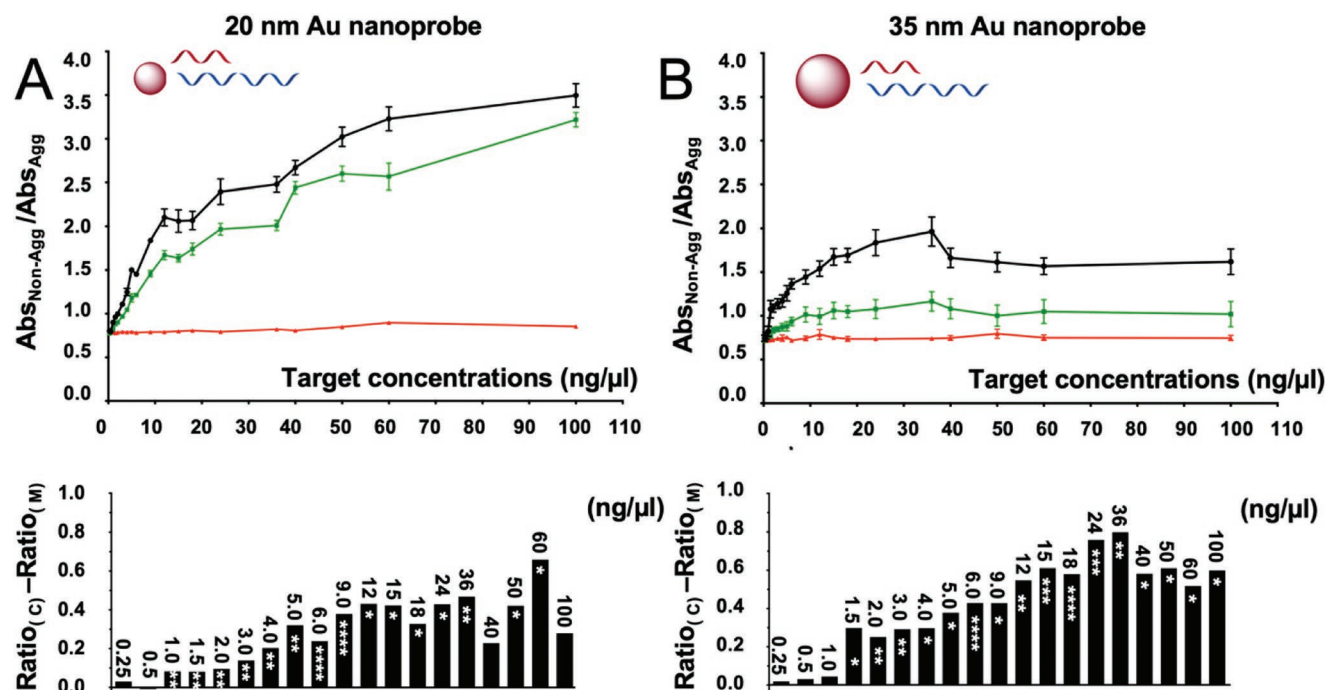


Figure 4. DNA concentration dependent effect of the aggregation ratio for A) 20 nm and B) 35 nm Au nanoprobe using three different 40-mer targets: totally complementary (black lines), mismatch (green lines), and totally noncomplementary (red lines). The bar graphs represent differences in aggregation ratios between complementary (C) and mismatched (M) targets, with one asterisk indicating  $p \leq 0.05$ , two  $p \leq 0.01$ , three  $p \leq 0.001$ , and four asterisks indicating  $p \leq 0.0001$  in cases of statistical significance.

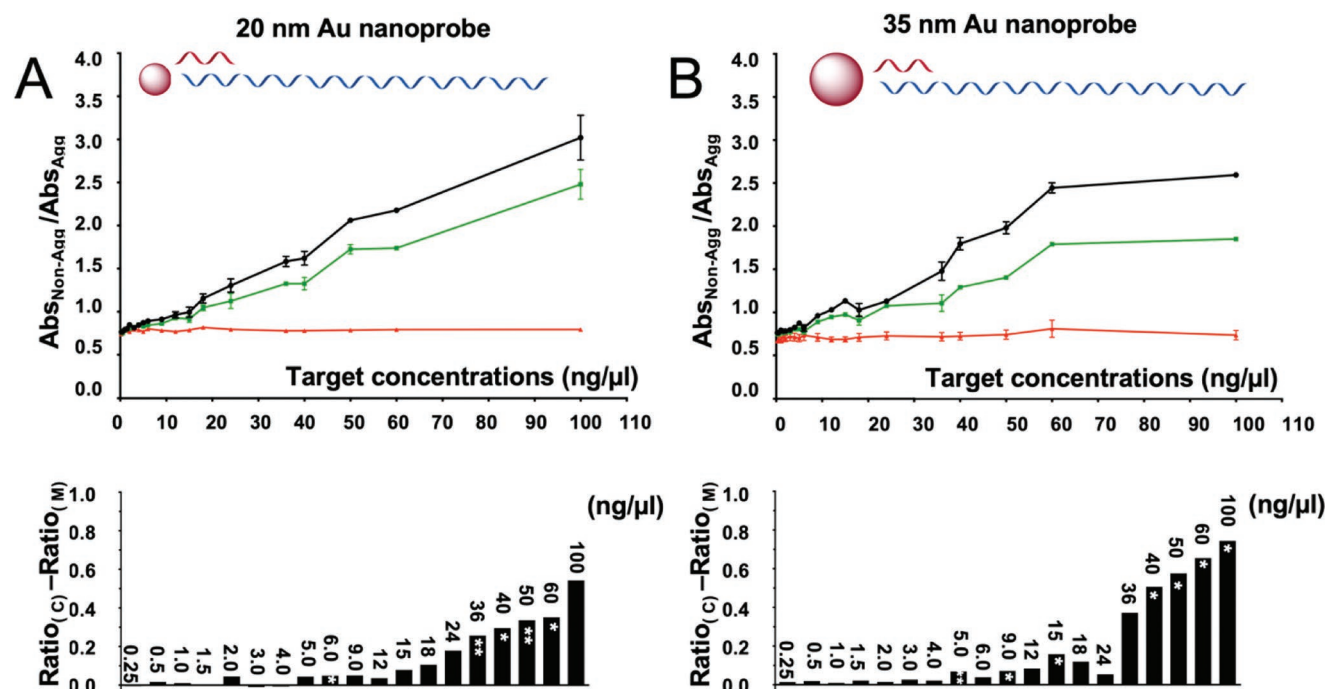


Figure 5. DNA concentration dependent effect of the aggregation ratio for A) 20 nm and B) 35 nm Au nanoprobe using three different 120-mer targets: totally complementary (black lines), mismatch (green lines), and totally noncomplementary (red lines). The bar graphs represent differences in aggregation ratios between complementary (C) and mismatched (M) targets, with one asterisk indicating  $p \leq 0.05$ , two  $p \leq 0.01$ , three  $p \leq 0.001$ , and four asterisks indicating  $p \leq 0.0001$  in cases of statistical significance.

and 5). This behavior is observed for both targets and both AuNP sizes and it is related to the increase in the number of dsDNA molecules formed per AuNP, increasing steric hindrance against salt-induced aggregation. As expected, more aggregation is observed for the mismatched sample in comparison with complementary samples, as Au nanoprobe should fully hybridize with the complementary DNA target, whilst hybridization with the mismatched DNA target is only partial, missing the last terminal base in the 20-mer probe. The difference between the extent of aggregation in the presence of the complementary target and the presence of the mismatched target is the basis of the discrimination of the assay, that is, the larger this difference, the better the discrimination. For the noncomplementary sample, as no hybridization occurs between target DNA and Au nanoprobe, there is no DNA concentration-dependent effect, and consequently, ratios do not significantly change by varying DNA concentration (red lines in Figures 4 and 5).

### 2.2.1. Detection Using a 40-mer Synthetic DNA Target

Figure 4 shows the results for 20 and 35 nm Au nanoprobe, using a 40-mer synthetic DNA target with concentrations up to 100 ng  $\mu\text{L}^{-1}$ . The line graphs represent aggregation ratios for three different targets: totally complementary (black lines), mismatched (green lines), and totally noncomplementary (red lines). The bar graphs in Figure 4 represent differences in aggregation ratios between assays with complementary and mismatched targets, a measure of the discrimination of the assay, for 20 nm (Figure 4A) and 35 nm Au nanoprobe (Figure 4B).

In Figure 4, a concentration-dependent protection against aggregation can be noticed for complementary and mismatch targets with an increase in the corresponding ratios with an increase in the DNA target concentration, independent of the size of the Au nanoprobe. For the noncomplementary sample, there is no concentration-dependent effect, as the ratios do not differ significantly between the different DNA concentrations. Therefore, different aggregation profiles can be seen between complementary or mismatched DNA and noncomplementary ones. This would be expected as the total complementary and the mismatch hybridize (totally or partially) with the Au nanoprobe protecting against aggregation induced by  $\text{MgCl}_2$ . The effect seems to be more significant for the complementary DNA compared to the mismatch. Even more important, different ratio curves describe a different aggregation profile also between complementary and mismatch DNA. The DNA concentration-dependent effect of the ratio between the maximum extinction coefficient of non-aggregated versus aggregated AuNP was previously reported for small 13–14 Au nanoprobe.<sup>[8,32]</sup>

Differences in aggregation ratios with statistical significance can be observed between complementary and mismatched targets, starting at a concentration of 1 ng  $\mu\text{L}^{-1}$  for 20 nm Au nanoprobe ( $**p \leq 0.01$ ), and starting at a concentration of 1.5 ng  $\mu\text{L}^{-1}$  for 35 nm Au nanoprobe ( $*p \leq 0.05$ ), assuring the discrimination of our assay for all target concentrations at or above those concentration values for each respective Au nano-

probe (see Supporting Information for a detailed analysis of the statistical significance of the differences observed).

Comparing the bar graphs from Figure 4A,B, it can be concluded that the assay discrimination is larger when 35 nm Au nanoprobe are used in the 40-mer target compared to 20 nm Au nanoprobe, especially for low target DNA concentrations, namely between 1.5 and 36 ng  $\mu\text{L}^{-1}$ .

### 2.2.2. Detection Using a 120-mer Synthetic DNA Target

Figure 5 presents results for the assay using a 120-mer target. Relative to the 40-mer target, the differences between aggregation ratios observed in totally complementary and mismatch targets are smaller, and they increase with target concentration (Figure 5A for 20 nm Au nanoprobe, and 5B for 35 nm Au nanoprobe). As observed for the shorter target, discrimination between complementary and mismatch targets is better for 35 nm Au nanoprobe than for 20 nm Au nanoprobe.

The lower discrimination capacity for longer targets was to be expected, as a point mutation in a sequence containing 40 bases represents 2.5% of the complete sequence, while the same point mutation in a sequence with 120 bases represents only 0.83% of that complete sequence. Different discrimination limits for DNA targets of different lengths were previously reported by Iglesias et al. using 65 nm Au nanoprobe to discriminate SNPs using 70 and 140 bp length DNA targets, with a limit of discrimination of 0.1 nmol  $\text{dm}^{-3}$  for the 70 bp DNA and 5 nmol  $\text{dm}^{-3}$  for the 140 bp DNA target.<sup>[40]</sup>

For 20 nm AuNPs, aggregation ratios for the three types of DNA targets are very similar for concentrations below 18 ng  $\mu\text{L}^{-1}$ , (Figure 5A). Discrimination between the complementary and mismatch targets only reaches statistical significance at 6 ng  $\mu\text{L}^{-1}$  ( $*p \leq 0.05$ ). These lower differences were expected, as the number of bases is three times higher in the 120-mer versus the 40-mer, and therefore, the same concentration in ng  $\mu\text{L}^{-1}$  corresponds to a lower number of single DNA strands for the 120-mer.

For 35 nm AuNPs, discrimination between the complementary and mismatch target DNA reaches statistical significance ( $*p \leq 0.05$ ) at a concentration of 5 ng  $\mu\text{L}^{-1}$  ( $*p \leq 0.05$ ). Some exceptions can be found at higher concentrations due to high variability amongst replicates (see Figure S9, Supporting Information, for a detailed analysis of the statistical significance of the differences observed).

### 2.2.3. Comparison with Other AuNP-Based SNP Assays

**Table 1** shows a comparison between our results and other similar SNPs assays. Limits of discrimination (LoD) for SNPs detection were reported to be down to 5 nmol  $\text{dm}^{-3}$  for a 41-mer target DNA and 13 nm Au nanoprobe, but the same experimental protocol failed to discriminate when applied to biological samples.<sup>[32]</sup> Larger 65 nm Au nanoprobe presented a similar LoD (5 nmol  $\text{dm}^{-3}$ ), but for a longer target DNA (140-mer) through a sandwich assay.<sup>[40]</sup> These limits are lower compared to the ones found in our study, which were  $\approx 165$  and 135 nmol  $\text{dm}^{-3}$  when using the 120-mer target, for 20 and 35 nm Au nanoprobe, respectively.

**Table 1.** SNP detection systems based on the aggregation of Au nanoprobe.

Au nanoprobe		Target		SNP discrimination limit	Reference
Size of spherical AuNPs	Oligo length/modification	Type	Length		
20 nm	20-mer ssDNA thiol C6 modification	Synthetic DNA	40 mer	1 ng $\mu\text{L}^{-1}$ (27 nmol $\text{dm}^{-3}$ )	This study
20 nm	20-mer ssDNA thiol C6 modification	Synthetic DNA	120 mer	6 ng $\mu\text{L}^{-1}$ (165 nmol $\text{dm}^{-3}$ )	This study
35 nm	20-mer ssDNA thiol C6 modification	Synthetic DNA	40 mer	1.5 ng $\mu\text{L}^{-1}$ (40 nmol $\text{dm}^{-3}$ )	This study
35 nm	20-mer ssDNA thiol C6 modification	Synthetic DNA	120 mer	5 ng $\mu\text{L}^{-1}$ (135 nmol $\text{dm}^{-3}$ )	This study
13 nm	Two ssDNA probes w/different lengths (21-mer; 2nd 20-mer)	Synthetic DNA	41 mer	5 nmol $\text{dm}^{-3}$ (no statistical analysis)	[32]
65 nm	Mut and WD ssDNA (20 and 23 mer) thiol-C6 modification	Synthetic DNA	70 mer	0.100 nmol $\text{dm}^{-3}$ (no statistical analysis)	[40]
65 nm	Mut and WD ssDNA (20 and 23 mer) thiol-C6 modification		140 mer	5 nmol $\text{dm}^{-3}$ (no statistical analysis)	[40]
14 nm	20 mer thiol-modified	PCR products	225 bp	30 ng $\mu\text{L}^{-1}$ (statistically significant)	[8]

On the other hand, Carlos et al.<sup>[8]</sup> developed a non-cross-linking assay, technically similar to ours, but using 14 nm Au nanoprobe. Their target was the SNP associated with fat mass and obesity-associated gene and they determined a limit of discrimination for the wild-type genotype, the heterozygous and fully mutated genotype of 30 ng  $\mu\text{L}^{-1}$ , much higher than ours (6 ng  $\mu\text{L}^{-1}$  for the 20 nm Au nanoprobe and 120 bp). The DNA targets used in their study were PCR products of 225 bp length that could be responsible for the relatively high limit of discrimination. Their study is one more example of the high variability described in the literature, underscoring the need for comparison studies, such as the one we present.

In addition to similar or better discrimination using 35 nm Au nanoprobe, it should be noticed that 35 nm nanoparticles allow a decrease in the cost/assay in comparison to 20 nm Au nanoprobe. Since the concentration used in the assays is 0.15 nmol  $\text{L}^{-1}$  for 35 nm Au nanoprobe and 2.5 nmol  $\text{L}^{-1}$  for 20 nm Au nanoprobe, there is an overall decrease of 80% in the amount of gold used and a decrease of 48% in the amount of oligonucleotide necessary for functionalization.

### 3. Conclusions

In summary, 20 and 35 nm Au nanoprobe were successfully functionalized using a salt aging or a pH method, respectively. The two distinct Au nanoprobe obtained using different functionalization ratios (150 and 1300, respectively) were used in different concentrations (2.5 nmol  $\text{dm}^{-3}$  for 20 nm Au nanoprobe and 0.15 nmol  $\text{dm}^{-3}$  for the 35 nm Au nanoprobe) and have demonstrated their ability to distinguish between total complementary, mismatch, and non-complementary DNA in the proposed experimental conditions. A thorough characterization of the aggregation state of the probes after functionalization, including the use of NTA, allowed us to choose the best experimental procedures and obtain Au nanoprobe with the required colloidal stability.

Overall, the discrimination was more efficient for the 40-mer ssDNA targets compared to larger 120-mer ssDNA

targets. Minimum target concentrations, at which discrimination between the mismatch and total complementary 20 and 35 nm Au nanoprobe becomes statistically significant, were 1 and 2 ng  $\mu\text{L}^{-1}$ , respectively. For the larger 120-mer targets, these lower limits were higher as statistical differences started to appear from 6 and 5 ng  $\mu\text{L}^{-1}$ , using 20 and 35 nm Au nanoprobe, respectively. This lower discrimination capacity for longer targets was to be expected, as a point mutation in a larger sequence impact much less the hybridization compared to the same point mutation in a three times shorter sequence.

As the difference between the complementary and mismatch DNA was overall much higher when using 35 nm Au nanoprobe compared to smaller 20 nm counterparts and independent of the length of the target, it can be concluded that 35 nm Au nanoprobe have a high potential for future detection assays, while decreasing the assay cost.

### 4. Experimental Section

**Synthesis and Characterization of AuNPs:** Smaller AuNPs (20 nm) were prepared by the citrate reduction method described by Ojea-Jiménez et al. and larger AuNPs (35 nm) were synthesized using a seed-mediated method described by Bastus et al.<sup>[41,42]</sup> Briefly, for 20 nm AuNPs, 2 mL of 343 mmol  $\text{dm}^{-3}$  trisodium citrate was added to 98 mL of 99 milli-Q water under heating while stirring in a round-bottom flask. 69.2  $\mu\text{L}$  of 1 mmol  $\text{dm}^{-3}$  HAuCl<sub>4</sub> were quickly added and the mixture was refluxed for 5 min with continuous stirring. The flask was cooled down to room temperature and stored in the dark. For larger AuNPs, the previous solution was used as seeds for growing the AuNPs. The solution was then heated to 90 °C, 1 mL of 25 mmol  $\text{dm}^{-3}$  HAuCl<sub>4</sub> was added, and the mixture was refluxed for 30 min with continuous stirring. Two more additions were necessary for obtaining the desired final diameter as assessed by UV-vis measurements. Both AuNPs were characterized by UV-vis spectroscopy (Figure 2) and transmission electron microscopy (TEM) (Figures S1 and S2, Supporting Information). Stock concentrations and size diameter were calculated accordingly to the method of Haiss et al. from the UV-vis spectra.<sup>[27]</sup> The stock concentrations were 8 and 0.22 nmol  $\text{dm}^{-3}$  for 20 and 35 nm AuNPs, respectively. The size distribution for the two stocks was evaluated through TEM analysis (Figures S1 and S2, Supporting Information).

**Synthesis and Characterization of Au Nanoprobe:** All unmodified and thiol-modified ssDNA oligonucleotides were purchased from



**Table 2.** Sequences of thiol-modified oligonucleotides used for AuNPs functionalization and of synthetic DNA targets.

Oligonucleotide	Length [bp]	Sequence 5' to 3'
Thiol-modified oligonucleotide	20	SH-C6- AGT TCC TTT GAG GCC AGG GG
Total Complementary DNA (CC)	40	ATA CAG ATA AGA TAA TGT AGC CCC TGG CCT CAA AGG AAC T
	120	CTT AGA CCC TAC AAT GTA CTA GTA GGC CTC TGC GCT GGC AAT ACA GAT AAG ATA ATG TAG CCC CTG GCC TCA AAG GAA CTC TCC TCC TTA GGT TGC ATT TGT ATA ATG TTT GAT TTT TAG
Mismatch (TT)	40	ATA CAG ATA AGA TAA TGT AGT CCC TGG CCT CAA AGG AAC T
	120	CTT AGA CCC TAC AAT GTA CTA GTA GGC CTC TGC GCT GGC AAT ACA GAT AAG ATA ATG TAG TCC CTG GCC TCA AAG GAA CTC TCC TCC TTA GGT TGC ATT TGT ATA ATG TTT GAT TTT TAG
Noncomplementary	40	TCC CGA GTT TCT TGT TAG ATT TTT AGT TTG TAA TAT GTT T
	120	TTC TAC CCT GCG AAC TTA CGG GAA AGC ATG ATG AGG GGA AAA TGG AGC AAT TAT GGG TGA CTG GAT AGG AGC ACC TTA CGT CCC GAG TTT CTT GTT AGA TTT TTA GTT TGT AAT ATG TTT

The discriminating nucleotide for the SNP of interest was located at the 3' end of the thiol-modified oligonucleotide and in the middle of the DNA targets.

Eurofins Genomics (Europe), except for the 40 bp DNA targets that were synthesized by STAB Vida, Lda. (Portugal). The discriminating nucleotide for the SNP of interest was located at the 3' end of the thiol-oligonucleotide (Table 2). For the functionalization of the 20 nm AuNPs, five different DNA:AuNP ratios: 50, 100, 150, 200, and 250 were used. Gold-nanoprobes were prepared by incubating the 20-mer thiol-modified ssDNA oligonucleotide with AuNPs for 2 h using the salt-aging method where NaCl (up to 0.1 M) was gradually added to increase DNA loading over 20 h.<sup>[26]</sup> Solutions were then washed by centrifugation at 15000 g for 10 min and resuspended in 10 mmol dm<sup>-3</sup> phosphate buffer (pH 8). 35 nm AuNPs were functionalized through a pH method using six different oligonucleotide:AuNPs ratios (400, 800, 1000, 1300, 1500, and 2000). Briefly, 35 nm AuNPs were initially concentrated through centrifugation at 800 g for 15 min, followed by incubation with oligonucleotide for 1 h. Eight microliters of 500 mmol dm<sup>-3</sup> pH 3 citrate/citric acid buffer were gradually added to the colloidal suspension and incubated for 1 h. Finally, the mixture was washed by centrifugation at 800 g (10 min) and resuspended in 10 mmol dm<sup>-3</sup> phosphate buffer (pH 8). All solutions were stored in the dark at 4 °C while in use. UV-vis spectroscopy was routinely performed while characterization with DLS and gel agaroses in the first optimization steps.

**UV-Vis Analysis:** All extinction spectra were performed in a UV-vis spectrophotometer (Spectrophotometer Cary 50 Bio UV-Visible, Varian) using quartz cells with a 1 cm path length (Hellma), at a wavelength ranging from 400 to 800, at room temperature. Unless stated otherwise, the UV-vis spectra were performed for the 20 nm at a concentration of 2 nmol dm<sup>-3</sup> while for the 35 nm AuNPs at a concentration of 0.1 nmol dm<sup>-3</sup>.

**Dynamic Light Scattering and Electrophoretic Light Scattering:** Measurements of hydrodynamic diameter and zeta potential for the AuNPs stock suspensions and Au nanoprobes were performed using a Malvern Zetasizer Nano ZS (Malvern, UK). An average of five measurements for each sample were taken at 25 °C, with light detection at 173° (DLS) and 17° (ELS). Measurements were performed at a final concentration of 8 and 0.22 nmol dm<sup>-3</sup> for 20 and 35 nm AuNPs suspensions, respectively. The Au nanoprobes were diluted 1 to 4 with 10 mmol dm<sup>-3</sup> phosphate buffer pH 8 just before the measurements.

**Nanoparticle Tracking Analysis:** Size distribution charts were obtained using a Malvern Analytical NanoSight NS300 (Malvern, UK) equipped with a 642 nm laser. Data acquisition and analysis were performed using the NTA 3.3 software. In the video acquisition step, they recorded ten videos of 60 s each, in ten distinct portions of the sample. Each video was then analyzed independently, and the results were merged into a single distribution.

**Transmission Electron Microscopy:** Micrographs were obtained using a JEM-1400 (JEOL) microscope, at Histology and Electron Microscopy Service (HEMS), Instituto de Investigação e Inovação em Saúde (i3S), Universidade do Porto, Portugal.

**Gel Electrophoresis:** Agarose gel 0.3% w/v was prepared by dissolving agarose in 1:8 TAE (pH 8.0). After jellification, 10 µL samples were added to each lane, and the gel was run at 120 V for 20 min in the same running buffer. An Apple iPhone 11 camera was used to photograph the gel after the run, registering the relative positions of the AuNP-derived bright red bands.

**Colorimetric Detection of the SNP Using Synthetic DNA:** The colorimetric detection was based on a non-cross-linking method where 20 and/or 35 nm Au nanoprobes were added in a final concentration of 2.5 (20 nm nanospheres) or 0.15 nmol dm<sup>-3</sup> (35 nm nanospheres) to a 10 mmol dm<sup>-3</sup> phosphate buffer pH 8 solution containing the synthetic DNA target. Three samples were used corresponding to a total complementary sequence to the Au nanoprobe, a mismatch, and a total noncomplementary DNA sequence to the Au nanoprobes. Two different lengths for the DNA target were tested at 40 and 120 bp in a final concentration ranging from 0.25 to 100 ng µL<sup>-1</sup>. Assay mixtures were heated at 75 °C and left to cool down at room temperature for 10 min for optimal hybridization. Then, MgCl<sub>2</sub> was added to evaluate the aggregation behavior of the Au nanoprobes in the presence of different DNA targets. After 10 min of reaction time at room temperature, all samples were analyzed visually and by UV-vis spectroscopy. A Blank was used containing the Au nanoprobe and the MgCl<sub>2</sub> salt in the corresponding concentration (no DNA target) and another control "Au nanoprobe" containing the Au nanoprobe alone (no salt, no DNA target).

To assess the colorimetric response, the UV-vis spectra of each sample were recorded. The spectrum of the non-aggregated sample (Au nanoprobe) was subtracted from the spectrum of the aggregated sample (blank control) and the minimum and maximum extinction values were determined. The minimum value corresponds to the wavelength of the non-aggregated state whereas the maximum value corresponds to the wavelength of the aggregate state. These wavelengths were then employed for measuring the colorimetric response for each sample as the ratio of the extinction peak of the non-aggregated nanoparticles (the minimum) to the characteristic extinction peak of the aggregated nanoparticles (the maximum), that is,  $Abs_{\lambda_{non-aggregated}}/Abs_{\lambda_{aggregated}}$ .

**Statistical Analysis:** All statistical calculations were performed using the GraphPad Prism 9 software (GraphPad Software, San Diego, CA, USA). Results are presented as mean ± standard deviation (SD) from at least three independent experiments. CC and TT samples were statistically compared by the unpaired student *t*-test. Normality of the data distribution was assessed by the Kolmogorov-Smirnov, D'Agostino & Pearson, and Shapiro-Wilk tests. Statistical comparisons between groups were performed by one-way analysis of variance (ANOVA) followed by Tukey's multiple comparison test, except when data did not follow the normal distribution. In this case, comparisons were made using the Kruskal-Wallis test followed by Dunn's post hoc test. Significance was accepted at *p* values <0.05.

## Supporting Information

Supporting Information is available from the Wiley Online Library or from the author.

## Acknowledgements

This work was financed by national funds from FCT – Fundação para a Ciência e a Tecnologia, I.P., in the scope of the following Projects: UIDP/04378/2020 and UIDB/04378/2020 of the Research Unit on Applied Molecular Biosciences – UCIBIO; LA/P/0140/2020 of the Associate Laboratory Institute for Health and Bioeconomy – i4HB; UIDB/50006/2020 and UIDP/50006/2020 of the Associate Laboratory for Green Chemistry – LAQV; and PTDC/NAN-MAT/30589/2017 (NANOMODE). Dr. Rocío Jurado is acknowledged for initial work under the scope of the NANOMODE Project.

## Conflict of Interest

The authors declare no conflict of interest.

## Data Availability Statement

The data that support the findings of this study are available from the corresponding author upon reasonable request.

## Keywords

DNA detection, gold nanoparticles, gold nanoprobe, lactose intolerance, molecular detection, non-cross-linking method, single nucleotide polymorphism

Received: July 22, 2022

Revised: October 1, 2022

Published online: November 9, 2022

- [1] Y. C. Yeh, B. Creran, V. M. Rotello, *Nanoscale* **2012**, *4*, 1871.
- [2] S. M. Shawky, A. M. Awad, W. Allam, M. H. Alkordi, S. F. El-Khamisy, *Biosens. Bioelectron.* **2017**, *92*, 349.
- [3] Y. Wang, X. Wang, X. Ma, Q. Chen, H. He, W. M. Nau, F. Huang, *Part. Part. Syst. Charact.* **2019**, *36*, 1900281.
- [4] P. Miao, Y. Tang, Z. Mao, Y. Liu, *Part. Part. Syst. Charact.* **2017**, *34*, 1600405.
- [5] M. P. de Almeida, E. Pereira, P. Baptista, I. Gomes, S. Figueiredo, L. Soares, R. Franco, in *Comprehensive Analytical Chemistry*, Vol. 66, Elsevier, New York **2014**, p. 529.
- [6] G. Doria, B. G. Baumgartner, R. Franco, P. V. Baptista, *Colloids Surf., B* **2010**, *77*, 122.
- [7] L. Soares, A. Csáki, J. Jatschka, W. Fritzsche, O. Flores, R. Franco, E. Pereira, *Analyst* **2014**, *139*, 4964.
- [8] F. F. Carlos, O. Flores, G. Doria, P. V. Baptista, *Anal. Biochem.* **2014**, *465*, 1.
- [9] T. M. Bayless, E. Brown, D. M. Paige, *Curr. Gastroenterol. Rep.* **2017**, *19*, 23.
- [10] C. L. Storhaug, S. K. Fosse, L. T. Fadnes, *Lancet Gastroenterol. Hepatol.* **2017**, *2*, 738.
- [11] D. M. Swallow, *Annu. Rev. Genet.* **2003**, *37*, 197.
- [12] C. C. Robayo-Torres, B. L. Nichols, *Nutr. Rev.* **2007**, *65*, 95.
- [13] G. Doria, R. Franco, P. Baptista, *IET Nanobiotechnol.* **2007**, *1*, 53.
- [14] G. Doria, M. Larginho, J. T. Dias, E. Pereira, R. Franco, P. V. Baptista, *Nanotechnology* **2010**, *21*, 255101.
- [15] P. Baptista, G. Doria, D. Henriques, E. Pereira, R. Franco, *J. Biotechnol.* **2005**, *119*, 111.
- [16] P. V. Baptista, M. Koziol-Montewka, J. Paluch-Oles, G. Doria, R. Franco, *Clin. Chem.* **2006**, *52*, 1433.
- [17] K. Sato, K. Hosokawa, M. Maeda, *J. Am. Chem. Soc.* **2003**, *125*, 8102.
- [18] M. Fujita, Y. Katafuchi, K. Ito, N. Kanayama, T. Takarada, M. Maeda, *J. Colloid Interface Sci.* **2012**, *368*, 629.
- [19] S. J. Hurst, A. K. Lytton-Jean, C. A. Mirkin, *Anal. Chem.* **2006**, *78*, 8313.
- [20] X. Zhang, T. Gouriye, K. Goeken, M. R. Servos, R. Gill, J. Liu, *J. Phys. Chem. C* **2013**, *117*, 15677.
- [21] X. Zhang, M. R. Servos, J. Liu, *J. Am. Chem. Soc.* **2012**, *134*, 7266.
- [22] C. A. Mirkin, R. L. Letsinger, R. C. Mucic, J. J. Storhoff, *Nature* **1996**, *382*, 607.
- [23] Z. He, S. Ding, L. Wang, G. Wang, X. Liang, T. Takarada, M. Maeda, *J. Chem. Educ.* **2021**, *98*, 3553.
- [24] J. J. Storhoff, R. Elghanian, C. A. Mirkin, R. L. Letsinger, *Langmuir* **2002**, *18*, 6666.
- [25] R. Gill, K. Göeken, V. Subramaniam, *Chem. Commun.* **2013**, *49*, 11400.
- [26] P. Valentini, R. Fiammengo, S. Sabella, M. Gariboldi, G. Maiorano, R. Cingolani, P. P. Pompa, *ACS Nano* **2013**, *7*, 5530.
- [27] W. Haiss, N. T. Thanh, J. Aveyard, D. G. Fernig, *Anal. Chem.* **2007**, *79*, 4215.
- [28] J. Lacava, A. Weber, T. Kraus, *Part. Part. Syst. Charact.* **2015**, *32*, 458.
- [29] G. Wang, Y. Akiyama, S. Shiraishi, N. Kanayama, T. Takarada, M. Maeda, *Bioconjugate Chem.* **2017**, *28*, 270.
- [30] J. Song, Z. Li, Y. Cheng, C. Liu, *Chem. Commun.* **2010**, *46*, 5548.
- [31] F. F. Carlos, B. Veigas, A. S. Matias, G. Doria, O. Flores, P. V. Baptista, *Biotechnol. Rep.* **2017**, *16*, 21.
- [32] W. Zhou, J. Ren, J. Zhu, Z. Zhou, S. Dong, *Talanta* **2016**, *161*, 528.
- [33] Y. Wang, J. Guo, Y. Guo, X. Zhang, H. Ju, *Sens. Actuators, B* **2018**, *267*, 328.
- [34] D. Feng, Y. Zhang, W. Shi, X. Li, H. Ma, *Chem. Commun.* **2010**, *46*, 9203.
- [35] Y.-S. Borghei, M. Hosseini, M. Dadmehr, S. Hosseinkhani, M. R. Ganjali, R. Sheikhejad, *Anal. Chim. Acta* **2016**, *904*, 92.
- [36] W. Zhao, W. Chiuman, M. A. Brook, Y. Li, *ChemBioChem* **2007**, *8*, 727.
- [37] C.-C. Chang, C.-P. Chen, C.-Y. Chen, C.-W. Lin, *Chem. Commun.* **2016**, *52*, 4167.
- [38] X. Ma, X. Kou, Y. Xu, D. Yang, P. Miao, *Nanoscale Adv.* **2019**, *1*, 486.
- [39] H. Kim, M. Park, J. Hwang, J. H. Kim, D. R. Chung, K. S. Lee, M. Kang, *ACS Sens.* **2019**, *4*, 1306.
- [40] M. Sanromán-Iglesias, C. H. Lawrie, L. M. Liz-Marzán, M. Grzelczak, *Bioconjugate Chem.* **2017**, *28*, 903.
- [41] I. Ojea-Jiménez, F. M. Romero, N. G. Bastús, V. Puntès, *J. Phys. Chem. C* **2010**, *114*, 1800.
- [42] N. G. Bastús, J. Comenge, V. Puntès, *Langmuir* **2011**, *27*, 11098.